JOURNAL OF GEOPHYSICAL RESEARCH, VOL. 97, NO. A11, PAGES 16,959–16,969, NOVEMBER 1, 1992

A New Method for Detecting the Projection of Magnetospheric Oscillations Into the Ionosphere

R. RAJARAM,[1] J. M. RUOHONIEMI, R. A. GREENWALD, AND K. B. BAKER

Applied Physics Laboratory, Johns Hopkins University, Laurel, Maryland

In situ magnetospheric observations and the corresponding data collected at the foot of the field line in the ionosphere can together form an invaluable tool for studying the processes involved in magnetosphere-ionosphere coupling provided the mappings between various regions in the magnetosphere and ionosphere are precisely known. A multivariate analysis technique is used to identify spatially localized modes of oscillations in the ionospheric plasma velocities monitored at F region heights by the Goose Bay HF radar. The temporal variations of these modes are compared with the magnetic fluctuations recorded by the AMPTE CCE satellite which was within the magnetic latitude-longitude region monitored by the radar. It is possible to clearly identify spatially localized modes in the ionosphere with temporal variations that track the azimuthal oscillations observed in the magnetosphere. This analysis approach offers a powerful method for establishing mappings between different regions of the magnetosphere and ionosphere under widely varying background conditions. The method, which is applied here exclusively to the mapping problem, can also be used to identify the natural modes of magnetospheric oscillation.

1. INTRODUCTION

Electrodynamic coupling between the magnetosphere and the ionosphere is affected by a number of driving and feedback processes acting over a wide range of spatial and temporal scales. Identification of these processes requires a precise mapping, along the geomagnetic lines of force, of specific regions in the magnetosphere and the ionosphere. This is usually achieved through integration of empirical models [*Stern and Alexeev*, 1987; *Tsyganenko*, 1987] which are based on magnetic field measurements carried out under widely different magnetospheric conditions. Apart from the fact that these models are handicapped by the very limited data available in the regions of the magnetosphere far removed from the equatorial plane, the magnetospheric field geometry is itself highly variable, depending on the state of magnetic activity. The development of diagnostic techniques for the determination of conjugate mappings between the magnetosphere and ionosphere is therefore of paramount importance. Such techniques can provide valuable checks on the accuracy of the empirical models and could form the basis of future time-dependent magnetospheric magnetic field models.

Identification of spatially localized hydromagnetic oscillations that are simultaneously monitored at magnetospheric and ionospheric heights can be used to generate conjugate mappings [*Greenwald et al.*, 1981]. Evidence for the existence of such local field line oscillations in the magnetosphere has been confirmed by a number of studies [*Lin et al.*, 1986; *Engebretson et al.*, 1986; *Anderson et al.*, 1990]. However, theoretical computations based on realistic ionospheric conductivities [*Southwood and Hughes*, 1983] show that localized signals are distorted and much is filtered by the ionosphere and prevented from reaching the ground (a mechanism that could account for the absence of any significant latitudinal dependence in the frequency of the observed ground magnetic pulsations). One has, therefore, to depend on observations above the E region of the ionosphere when looking for localized oscillations of magnetospheric origin.

Ground-based HF coherent radars can provide snapshot pictures of the motions of the F region plasma by monitoring the movement of small-scale (~10 m) electron density irregularities transverse to the field line over an area of $\sim 10^6$ m^2 with a time resolution of ~1 min and a spatial resolution of several tens of kilometers [e.g., *Ruohoniemi et al.*, 1991]. Owing to the relative ease with which magnetospheric electric fields of various spatial scale sizes can penetrate to the F region of the ionosphere, the oscillations in the motion appear as a superposition of modes with a wide range of spatial and temporal characteristics. A spatially localized mode of oscillation cannot, therefore, be isolated through a simple visual inspection. The technique utilized for the purpose has to be geared to identify, in the data set, patterns of spatial and temporal variations that are independent of each other.

A radar scan provides information on the line-of-sight motion of each of the regions from which it receives backscatter signals. Depending on the quality of the scatter, the number of such samples can vary. If the motion of the scatterers is random, the oscillations at different points will not be correlated. However, if the oscillations are driven by some specified (but unknown) number of modes, the individual motions will be correlated and all the information that is contained, in the plethora of individual motions, should, in principle, be expressible in terms of a much smaller number of oscillation modes. A number of sophisticated multivariate methods are available for efficient replacement of a large number of measurements by a smaller number of functions without the loss of much information. The simplest and most utilized of these is the so-called principal component analysis [*Rao*, 1965]. In the principal component analysis, the new variables are expressed as a linear combination of the old variables, and the coefficients are determined by minimizing the variance of the residuals. It often happens that the first few components account for most of the data, which aids the process of interpretation. In its original form, variables with zero mean were adopted, and the resultant principal components turned out to be the mutually orthogonal

[1]Permanently at Indian Institute of Geomagnetism, Colaba, Bombay, India.

Paper number 92JA00830.
0148-0227/92/92JA-00830$05.00

eigenvectors of the correlation or covariance matrix depending on whether the variables were normalized or not. Such a choice is not necessary, however, and it is often advantageous to work without discarding the additional information that the mean value of each variable can provide [*Faynberg*, 1975; *Rajaram*, 1980; *Rajaram and Rajaram*, 1983].

In the present study, we adopt the principal component analysis to identify modes of oscillation in the ionosphere and see whether the temporal variations of any of these matches the magnetic field oscillations recorded in the magnetosphere by a satellite which is within the field of view of the radar. The magnetic field measurements from the Active Magnetospheric Particle Tracer Explorers (AMPTE) CCE satellite are used for the magnetospheric component of the data base while the Doppler velocities obtained from the Johns Hopkins University/Applied Physics Laboratory (JHU/APL) HF radar at Goose Bay, Labrador (53.4°N, 60.4°W), which looks over northeastern Canada and Greenland, provide the ionospheric component. The data segments used have been necessarily confined to periods when the magnetic field line footpoint of AMPTE CCE was expected to be within the field of view of the Goose Bay radar. Such periods are fairly common, and the data base can be utilized for extensive statistical studies.

The AMPTE CCE carried a flux gate magnetometer system with seven automatically switchable ranges from ±16 nT to ±65,536 nT (full scale) and resolution commensurate with a 13-bit analog to digital converter in each range [*Potemra et al.*, 1985]. The sampling rate of the instrument was 8.06 vector values per second. The AMPTE CCE orbit is equatorial (4.8° normal inclination) with apogee at 8.8 R_E and perigee at 1000 km and a period of 15.6 hours. The range of magnetic latitudes covered is ±16°, and the orbit precessed westward at a rate of 0.77°/day.

The Goose Bay radar has been described in detail by *Greenwald et al.* [1985]. The phased array antenna scans a 52° azimuth sector centered on 5° east of geographic north with a narrow (~4°) beam. The antenna bore sight is swept in the clockwise direction through 16 evenly spaced pointing azimuths. The integration time for each beam position is typically 6 s. This is increased to 12 s when the radar receives on two arrays simultaneously (vertical interferometer mode). Thus complete scans require 96 or 192 s. The radar may be operated anywhere in the 8- to 20-MHz range, and for each azimuth, the returns from 50 range gates are sampled simultaneously. The gate separation is 45 km. The range to the first gate can be set to any value but is generally close to 200 or 600 km. The microcomputer calculates 17-lag complex autocorrelation functions; at the time of the experiment described in this paper only the autocorrelations for the 20 range gates that returned the most backscattered power were stored on tape. (With recent upgrades all autocorrelation functions are now saved on optical disk.) The lag-dependent phase of the complex autocorrelation functions is subsequently analyzed to determine the Doppler velocities associated with retained data. Thus Doppler velocities determined from successive radar scans may come from different spatial locations, and this has to be accounted for in the multivariate analysis.

Since the technique adopted by us is not very commonly used, a discussion of the basic methodology underlying the component analysis is presented in the next section. An account of the actual analytical procedure used, presentation of results, discussion, and our thoughts on future work can be found in the subsequent sections.

2. Methodology

The basic philosophy governing the multivariate analysis technique adopted here is to reduce, through an objective procedure, the number of variables required to account for the time variations present in the entire radar data set. Descriptions of the method can be found elsewhere [*Faynberg*, 1975; *Rajaram*, 1980; *Rajaram* and *Rajaram*, 1983], but a brief outline is presented here for the sake of clarity.

The basic data set consists of $n \times m$ values of $V(x_i, t_j)$, the Doppler velocities recorded at n locations x_i ($i = 1, \ldots n$) at m instants of time t_j ($j = 1, \ldots m$). We expand $V(x_i, t_j)$ in terms of mutually orthogonal functions which are derived from the statistical properties of the data itself. Thus

$$V(x_i, t_j) = \sum_{k=1}^{n} X_{ik}(x_i) T_{kj}(t_j) \tag{1}$$

where $X_{ik}(x_i)$ and $T_{kj}(t_j)$ satisfy

$$\sum_{i=1}^{n} X_{il} X_{ik} = \delta_{lk} \tag{2}$$

$$\sum_{j=1}^{m} T_{lj} T_{kj} = \lambda_k \delta_{lk} \tag{3}$$

We expand the velocity field $V(x_i, t_j)$ as a sum of n modes with each mode k being described by a spatial distribution function $X_{ik}(x_i)$ and a time variation $T_{kj}(t_j)$. The functions X_{ik} and T_{kj} are calculated through a least squares fit to the data of observed $V(x_i, t_j)$ subject to the constraints imposed by equations (2) and (3). It turns out that the X_{ik} ($i = 1, \ldots n$) are the eigenvectors of the matrix

$$\mathbf{R}_{il} = \sum_{j=1}^{m} V(x_i, t_j) V(x_l, t_j) \tag{4}$$

and are obtained as solutions of the eigenvalue problem

$$\sum_{l=1}^{n} \mathbf{R}_{il} X_{lk} = \lambda_k X_{ik} \tag{5}$$

$$T_{kj} = \sum_{i=1}^{n} V(x_i, t_j) X_{ik} \tag{6}$$

It is easy to see that $\mathbf{R}$ would correspond to the covariance matrix if the sample mean were zero and to the correlation matrix if, in addition, the variables were normalized so as to have unit variance.

In the component analysis, the eigenvectors X_{ik}($i = 1, \ldots n$ and $k = 1, \ldots n$) are arranged according to decreasing order of the eigenvalues λ_k. Thus the first eigenvector would correspond to the highest eigenvalue, the second to the next and so on. Since X_{ik} is normalized to unity by equation (2), equation (3) suggests that the mode corresponding to the highest eigenvalue will make the largest contribution to the observed V and the contributions will decrease with decreasing eigenvalues. Further, from equation (1), we note that the contribution of component k at position x_i and time t_j is given by $X_{ik} \times T_{kj}$, i.e., the contribution of mode k at position x_i multiplied by the amplitude of the mode at time t_j. The eigenvectors, X_{ik}, provide the spatial distribution of the line-of-sight velocities for a given mode, k, and thus the pattern of spatial variation associated

with the mode. The T_{kj}, on the other hand, show how the magnitude of the velocities associated with the flow varies with time. The quantity

$$P = \frac{\lambda_k}{\sum_{j=1}^{n} \lambda_j} \times 100 \tag{7}$$

is a measure of the percentage of the data accounted for by the component k.

The expansion described above is in essence a rotation of the vector of observations involving the replacement of the velocity at n different points by the amplitude of n different modes. The utility of the approach lies in the fact that if λ_k (and hence P) turns out to be a rapidly decreasing function of k only a few modes remain relevant, and the interpretation of the data becomes relatively easy provided we have a meaningful physical hypothesis. In our case this is provided by the independent measurement of fluctuations in the magnetosphere from the AMPTE CCE magnetometers.

3. Selection of the Event

The orbital parameters of the AMPTE CCE spacecraft were scanned for periods when it was within the field of view of the Goose Bay radar, and the interval from 0700 UT to 1000 UT on December 10, 1988, was chosen for the present analysis. Figure 1 shows the AMPTE CCE magnetic field data between 0500 UT and 1030 UT in cylindrical *VDH* coordinates. In this coordinate system, the H axis is chosen along the unit vector $\hat{\mathbf{h}}$ (positive north) antiparallel to the geomagnetic dipole (but parallel to the observed magnetic field at the equator), the D axis is along $\hat{\mathbf{d}}$ which is perpendicular to the local dipole meridian (positive eastward), and the V axis is directed along $\hat{\mathbf{v}}$ given by $\hat{\mathbf{v}} = \hat{\mathbf{d}} \times \hat{\mathbf{h}}$.

The figure depicts the variation along the satellite trajectory of BV, BD, and BH (the components of the magnetic field along the V, D, and H axes), BT (the total field strength), theta (the angle that the field makes with the equatorial plane), and phi (the azimuth of the field). The location of the satellite is shown at the bottom of the figure using the geocentric distance (R), magnetic latitude (MLAT), and the magnetic local time (MLT).

The satellite magnetic records show distinct pulsation activity during this period. The quality of the radar data for the period was also adequate and suitable for deducing ionospheric motions over a sizable region in the ionosphere. The geomagnetic conditions were moderately quiet (Kp = 1+) in the third 3-hour interval (0600–0900 UT), but there was an enhancement in the activity (Kp = 3+) in the next three hour period. The satellite was in the dawn sector moving out from 6.16 R_E at 0700 UT to 8.41 R_E at 1000 UT (compare Figure 1). The magnetic latitude was around 15°. The invariant latitude, computed on the basis of a dipole field model, varied from around 67° at 0700 UT to around 70.5° at 1000 UT. However, as the satellite moved toward greater radial distances, the local magnetic field observed by it changed from a compressed dipole to a taillike configuration.

4. Satellite Data

The analysis of the satellite data is fairly straightforward. We work with 6.2-s averages of the three components of the AMPTE CCE magnetic field data. In order to project the oscillations in terms of their transverse and longitudinal components, the magnetic fields are expressed in terms of field-aligned coordinates that we now define.

The background field geometry is derived from 20-min averages of the components of the measured magnetic field in geocentric solar ecliptic (GSE) coordinates. The spatial variation of the orientation, $\hat{\mathbf{b}}$, of the background magnetic field at the AMPTE CCE location appears as a secular trend and is obtained as $\mathbf{B}_0/|\mathbf{B}_0|$, where $\mathbf{B}_0$ is the estimated background magnetic field derived from the 20-min averages, $\langle \mathbf{B} \rangle$, through interpolation. From the orbit data, the location of the satellite is obtained which can then be used to define $\hat{\mathbf{r}}$, the unit vector along the radius vector to the satellite location. The field-aligned coordinates are defined by $\hat{\mathbf{b}}, \hat{\phi} = \hat{\mathbf{b}} \times \hat{\mathbf{r}}/|\hat{\mathbf{b}} \times \hat{\mathbf{r}}|, \hat{\mathbf{n}} = \hat{\phi} \times \hat{\mathbf{b}}$. A similar representation was adopted by *Takahashi et al.* [1990]. The main advantage in using such field-aligned coordinates is that the components along $\hat{\mathbf{b}}$, $\hat{\phi}$, and $\hat{\mathbf{n}}$ give directly the fluctuation in the magnitude of the magnetic field, ΔB, the azimuthal variation, D, and the transverse poloidal component, ΔB_R, respectively.

Since the sampling of the radar data in this experiment is not better than 1 min, the components of the magnetic field in the field-aligned coordinates are averaged every minute. Finally, the long-term trends are removed by subtracting out 20-min sliding averages. The resulting time series are used to represent the magnetospheric magnetic field fluctuations.

5. Radar Data

The analysis of the radar data is more involved. A typical scan can take 96 to 192 s, but for the purpose of this study, all the Doppler velocities obtained from a scan have to be referred to a single time, and only oscillations with time scales greater than about 5 min can provide reliable identification of spatial structure. But even within the limits imposed by these requirements, the analysis can provide very meaningful results.

We note that successive scans need not contain data from the same combination of azimuth and range gate or, in other words, the same location in the ionosphere. We first determine from all the scans in each specified interval the number of samples that correspond to each specific location defined by azimuth and range gate (assuming a constant height of backscatter). The locations can then be classified according to the number of scans for which data are available. Ideally, to avoid interpolation of data, only points represented in all the scans should be considered, but since this would reduce the number of points and possibly remove certain areas from the map, a compromise solution has been adopted. We have required that not more than 10% of the scans should be missing at any chosen location. In the present work, interpolation has been carried out only in time.

The analysis involves the following steps:

1. Data from all 16 azimuths and 50 range gates for each specified period were examined and a decision made as to the number of spatial locations, n, to be used in each interval. The intervals were chosen so as to encompass the three 1-hour intervals (0700–0800 UT, 0800–0900 UT and 0900–1000 UT) and to ensure the inclusion of all full scans. The periods were also varied around a bit to test for the stability of the analysis.

2. After fixing the value of n, interpolation in time was carried out to fill temporal gaps in the data at any chosen location. Interpolation could have been carried out using neighboring spatial points corresponding to the same time, but this was avoided in order not to bias the spatial structure determined by the analysis.

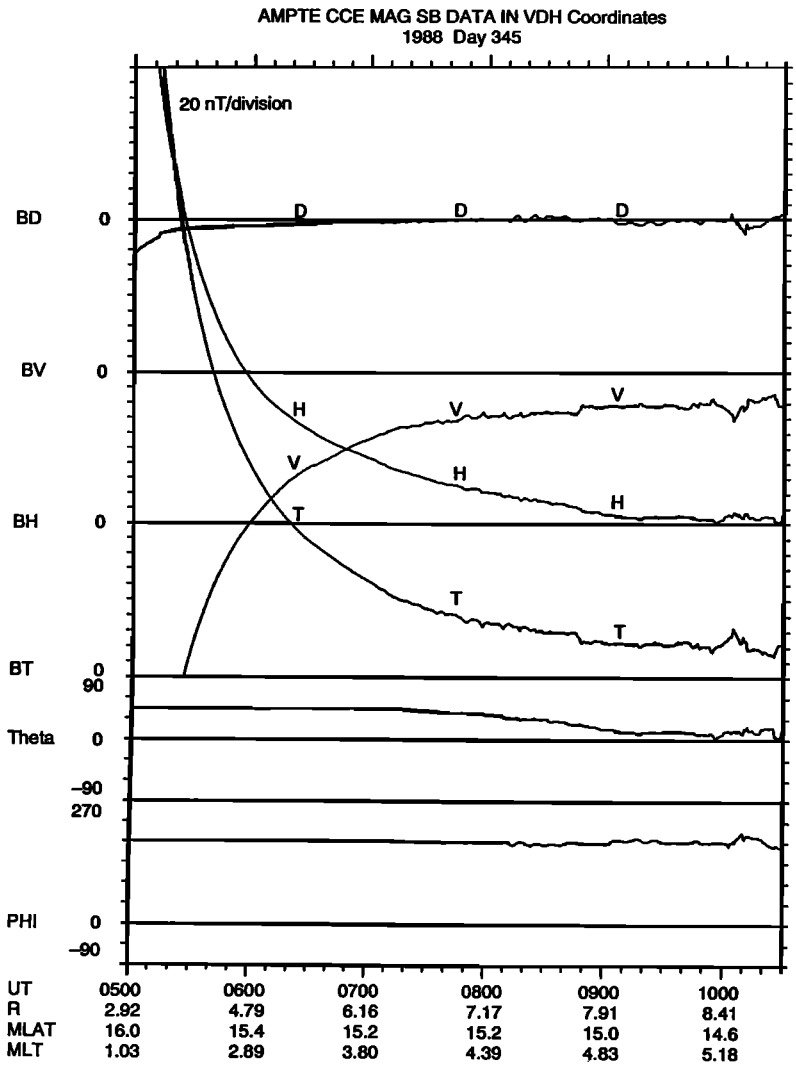

Fig. 1. AMPTE CCE magnetic field data in the *VDH* coordinates (described in the text) from 0500 UT to 1030 UT on December 10, 1988. The satellite position is given at the bottom of the figure.

3. The resulting multiple time series were then used to compute the "covariance matrix" **R** given by equation (4).

4. The matrix **R** was subjected to an eigenvector analysis, and eigenvectors were arranged according to decreasing eigenvalues.

5. The eigenvectors X_{ik} were then used to compute the time series of the components, T_{kj}, using equation (6) and the percentage of the variance accounted for was obtained from equation (7).

6. Finally, X_{ik} was subjected to the "L shell" method of velocity analysis (described by *Ruohoniemi et al.* [1989] for individual scans) to estimate the two-dimensional flows associated with each mode. A constant height of 300 km was assumed for the scattering region.

The results of the analysis are presented in the next section.

6. Results and Discussions

We provide, in this section, an explicit presentation of the results of the analysis described in the last section for three specific data intervals. These are specified by the time periods 0646:23–0804:51 UT, 0753:39–0902:30 UT, and 0851:17–1006:33 UT. The velocity data (obtained from the radar scans) were characterized by the presence of oscillations through the entire period. Figure 2 shows the time variations in 11 successive ranges (gates 15–25) of beam 8 for the period of interest. The large spatial variability present in the time series justifies the application of a principal component analysis.

In the first interval a total of 120 spatial locations were covered and 39 scans were included in the analysis with no point represented by less than 35 scans. The second and third intervals provided only 100 spatial locations with nearly contiguous data. The total number of scans were 35 and 38 in the second and third intervals and the minimum number of scans at any location were 32 and 34, respectively.

Figure 3 shows how the first eight components, T_{kj}, obtained for the first interval vary from 0700 UT to 0800 UT. Figure 4 depicts the two-dimensional flows associated with each of the components. These patterns are based on an analysis of the azimuthal variations in the line-of-sight radar measurements of the ionospheric drift [*Ruohoniemi et al.*, 1989]. Although there are potential problems with the procedure owing to unresolved curvature in the flow [*Freeman et al.*, 1991], we adopt this presentation to give a clear physical representation of the localization of the components in latitude, their amplitude, and likely orientation. The derivation of the components and their subsequent intercomparison with the satellite

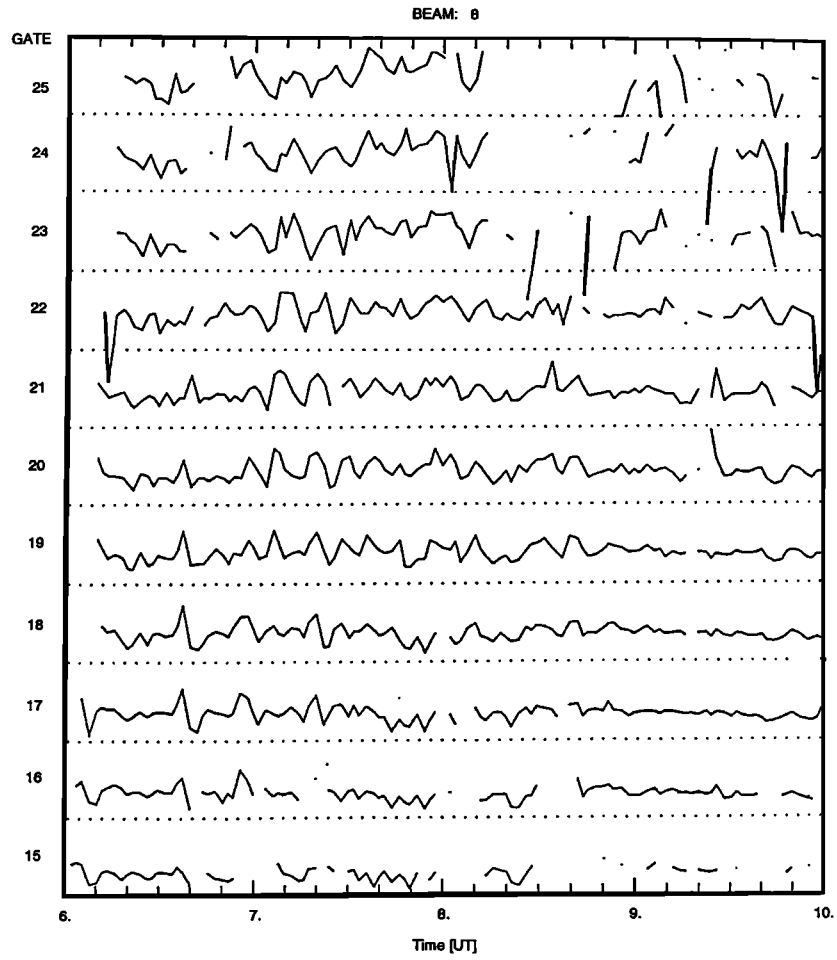

Fig. 2. Time variation of the radar line-of-sight velocities for range gates 15 through 25 of beam 8. The dotted lines constitute zero-velocity reference levels for the respective time series, and the separation of these lines represents a velocity step of 1000 m/s.

data are based on the line-of-sight radar data and hence are independent of any inaccuracy in the vector estimation. Also note that varying the assumed height of scattering within reasonable limits for F region scatter (250–400 km) shifts the patterns only slightly in latitude.

Component 1 reproduces the large-scale zonal flows along with their time variation. It accounts for 88% of the variability in the data and highlights the presence of large-scale global oscillations in the system. Note that when a component is negative in Figure 3, the observed flows will be directed in a direction opposite to that indicated in Figure 4. The variation could have also been represented by simultaneously reversing the signs of the flow vectors and component values. Such a symmetry follows directly from the representation adopted in equation (1) which is invariant under the simultaneous reversal of the signs of X_{ik} and T_{kj}.

Among the other components, the second accounts for 3.5%; the third, 1.3%; the fourth, 1%; the fifth, 0.8%; the sixth, 0.7%, the seventh, 0.65%, and the eighth, 0.5% of the data. These components represent spatially localized flows and therefore account only for a small percentage of the total variation present in the data. However, they contribute substantially to the oscillations within the localized regions where they have a significant presence. Note that component 5 makes significant contributions in two regions, one below 68.5° and the other around 78° latitude. The significance of this is not obvious. It is also worth noting that the frequencies of the temporal oscillations in components 5 and 8 are similar.

In order to determine whether the satellite records fluctuate with temporal characteristics similar to any of the components depicted in Figure 3, we look into the magnetic field variations recorded by AMPTE CCE. In Figure 5, we depict the magnetic field variations at the AMPTE CCE location along with the time variations of components 5 and 8. It is obvious from the figure that the oscillations in D are quite similar to those of component 8 through most of the period except for the very beginning, where it appears to match component 5 better. A tentative explanation will be offered for this at the end of this section. It should, however, be pointed out that it is only the nature of the temporal variations that matches. The amplitudes do not match as well. It should also be pointed out that the satellite was in motion, and the variations recorded by it could also have had a spatial component. It may, therefore, not be realistic to expect a perfect match.

As the amplitudes in the two series do not match from cycle to cycle, a correlation analysis is unlikely to do justice to the degree of similarity. However, for the sake of completeness, we have computed the cross correlation for various time lags. Since the AMPTE CCE magnetic field data are evenly and closely spaced in time, it is easy to obtain the values of D corresponding to the times of the radar measurements, or at specific lag or lead times with respect to it, by performing lin-

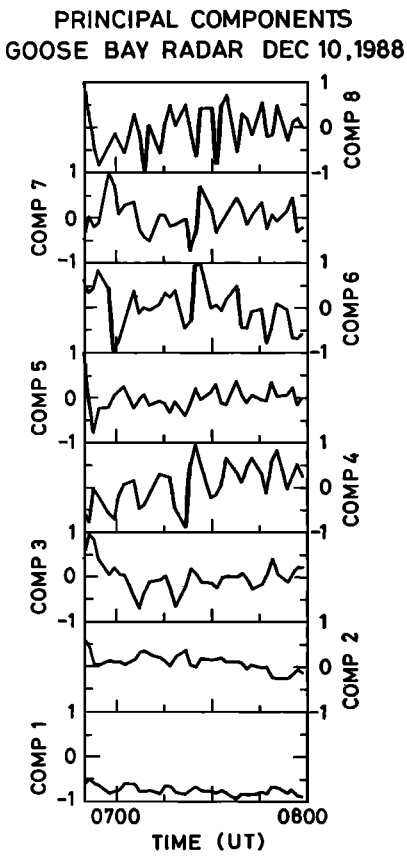

Fig. 3. Time variation of the first eight principal components of the ionospheric flow in the interval 0645 UT to 0800 UT.

ear interpolations. A visual inspection of the patterns in Figure 5 suggests significant similarities between the D variation and the component of the radar data in the period 0710 to 0800 hours UT. Cross correlations computed between the two series for this interval (which include 24 points) show that the correlation coefficient is around 0.67 at zero lag (significant at the 99% confidence level). Since the time series had a clear 6-min oscillation, significant negative correlations are present at lags of ±3 min and positive correlations at lags of ±6 min.

Before proceeding on to a discussion of the results obtained for the other data segments, it may be worthwhile making a few points on the authenticity of the components and their spatial structure. The technique is objective, and the time series corresponding to each channel is treated as an independent channel of information without any consideration of physical proximity. Thus if any component is determined only at the noise level, the velocity vectors at neighboring spatial locations will be unrelated and randomly oriented. The principal purpose of presenting the two-dimensional flows (such as shown in Figure 4) is to demonstrate how well ordered and well defined the spatial structures are. At the same time, as no physics have gone into the determination of the components (which have been defined by the spatio-temporal features of the data alone), the basic interpretation of the components is best achieved by linking them with a set of independent data (as we have done) or with the results of a model calculation. Certain broad comments can, however, be made: The first component shows that the ionospheric motions in the morning sector were dominated by large-scale eastward flows. Components 2 and 3 bring out the presence of significant flows at high latitudes that were re-

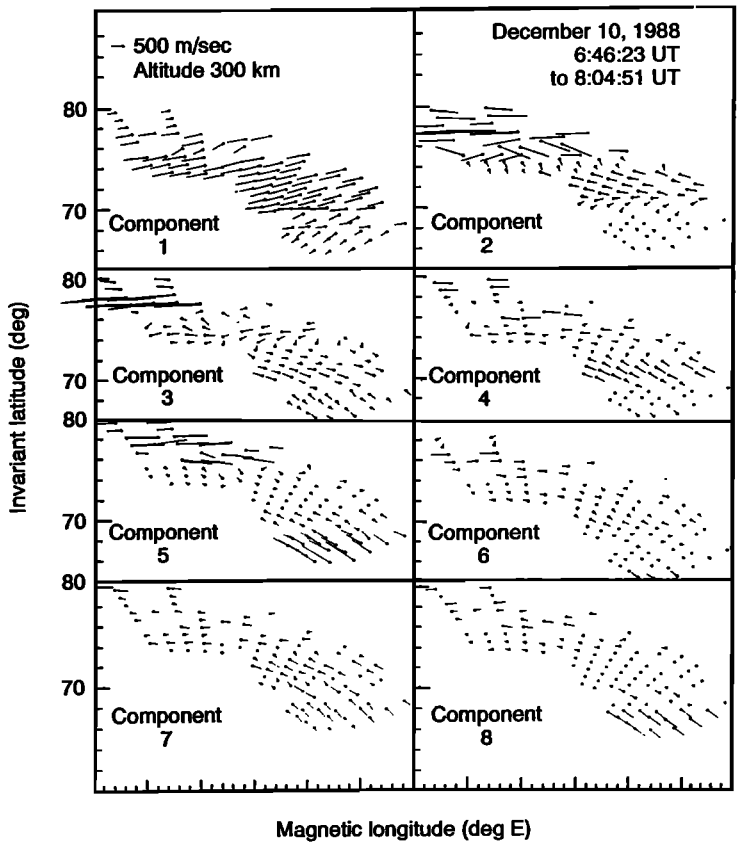

Fig. 4. Vector velocity maps obtained from the analysis of the spatial distributions corresponding to the first eight components of the radial velocity eigenvectors assuming uniformity of flows along L contours.

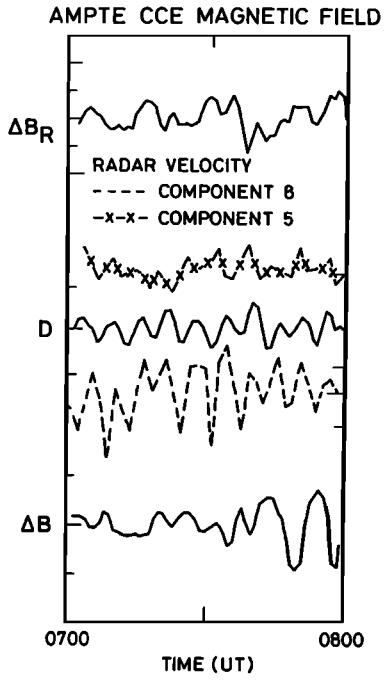

Fig. 5. Plots of the oscillations of the magnetic field strength (ΔB), transverse radial (ΔB_R), and transverse azimuthal (D) oscillations recorded by AMPTE CCE magnetometers along with the principal components 5 and 8 of the ionospheric flows for the time interval 0700 UT to 0800 UT.

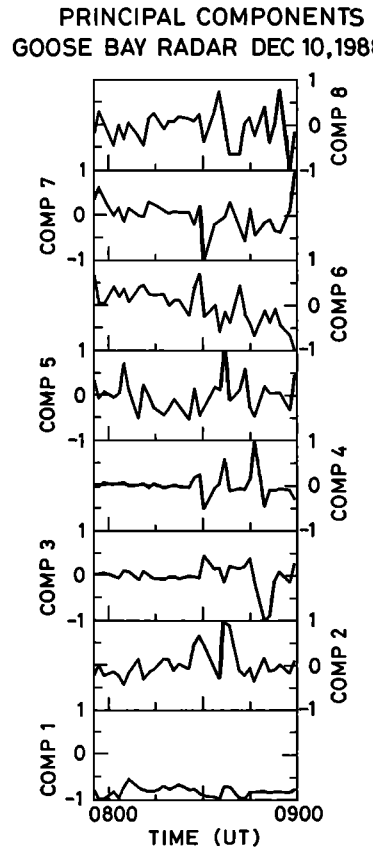

Fig. 6. Same as in Figure 3 except that it is plotted for the time interval 0750 UT to 0900 UT.

stricted in latitudinal extent. Component 8, which has been of primary interest to us, was apparently driven by toroidal oscillations in the magnetosphere. The corresponding ionospheric flows appear to have been tilted with respect to the azimuth. However, it may be difficult to assert that this is real and associated with rotation of the plane of polarization of the hydromagnetic wave as it propagates from the magnetosphere to the ionosphere [*Southwood and Hughes*, 1983], as one cannot rule out the possibility that such tilts could have been introduced by inaccuracies in the process of estimating the two-dimensional flows on the basis of line-of-sight velocities or by the inability of the analysis technique to precisely reproduce the spatial structure of the oscillations.

Figure 6 shows the time variations of the first eight components in the next interval, and Figure 7 shows how the satellite D variations reproduce many of the salient features in component 5, which accounts for about 0.9% of the total ionospheric flow oscillations. Though the match is not as dramatic as in the first interval, the conjugacy is quite apparent in the similarity of the temporal variations as indicated by the locations of the peaks. We emphasize again that the amplitude of the oscillation associated with a component that explains a relatively small percentage of the data can be quite substantial (as much as 500 m/s in this case) in the regions where they are significant. Figure 8 illustrates the spatial localization of the two-dimensional flows that are associated with component 5 in this interval. The correlation coefficients obtained for the interval (0800–0900 hours UT) show the largest magnitude (−0.44) when the radar velocity changes are correlated with the AMPTE CCE variations 6 min later. With 29 points in this data interval, the correlation is significant at the 98% confidence level.

Finally, in Figures 9–11 we examine the conjugacy of satellite and radar observations in the data interval 0900 UT to 1000 UT. Figure 9 shows the temporal variations in the first eight components of the ionospheric flow. We note from Figure 10 that component 4, which accounts for about 0.5% of the data, reproduces many of the salient features of the D varia-

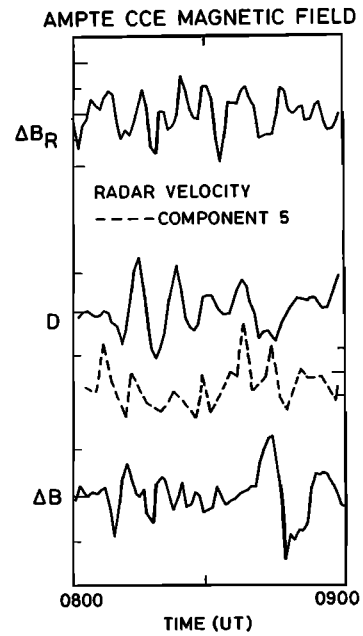

Fig. 7. AMPTE CCE magnetic field oscillations between 0800 UT and 0900 UT along with those of component 5 of the ionospheric flows obtained through the eigenvector analysis.

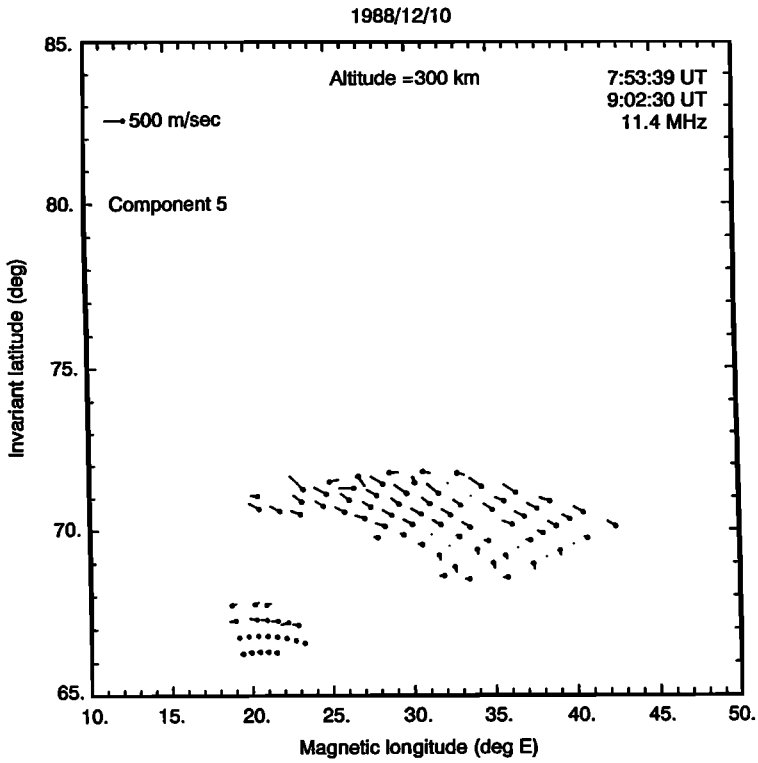

Fig. 8. Vector velocity maps of the ionospheric flows between 0750 UT and 0900 UT corresponding to component 5 whose time variations are depicted in Figures 6 and 7.

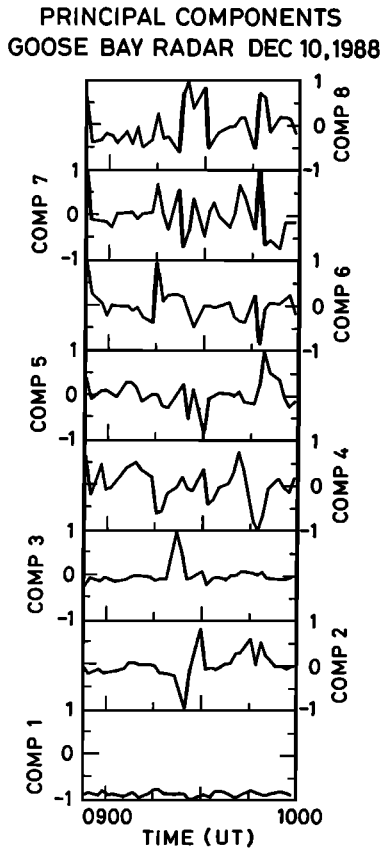

Fig. 9. Same as Figures 3 and 6 except that it is for the time interval 0850 UT to 1000 UT.

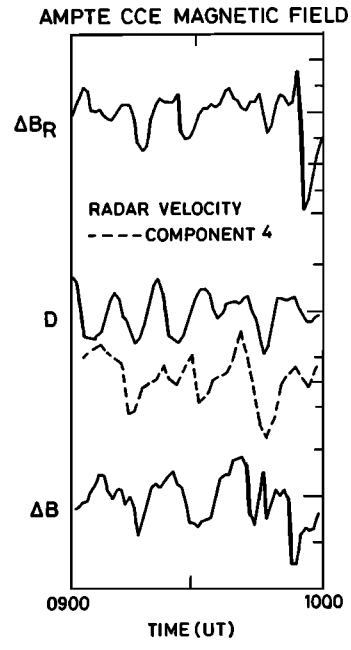

Fig. 10. AMPTE CCE magnetic field oscillations between 0900 UT and 1000 UT along with those of component 4 of the ionospheric flows obtained through the eigenvector analysis.

tions recorded by the AMPTE CCE magnetometer except for a small period at the beginning of the interval. Figure 11, which depicts the spatial distribution of the flows associated with component 4 in this interval, shows that the mode is extremely localized in its latitudinal extent. It is quite conceivable that the satellite was not in the region where these oscillations were

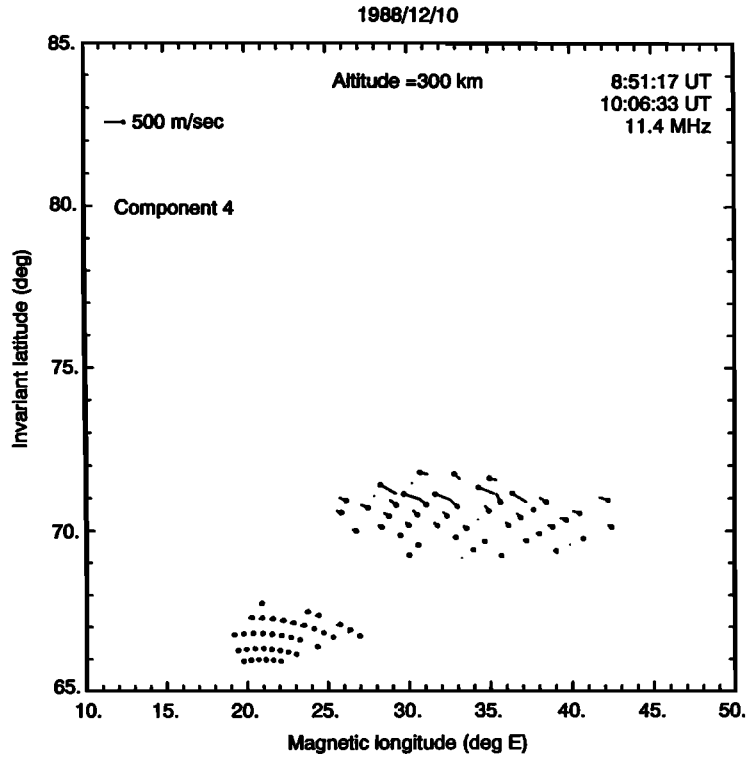

Fig. 11. Vector velocity maps of the ionospheric flows 0850 UT to 1000 UT corresponding to component 4 whose time variations are depicted in Figures 9 and 10.

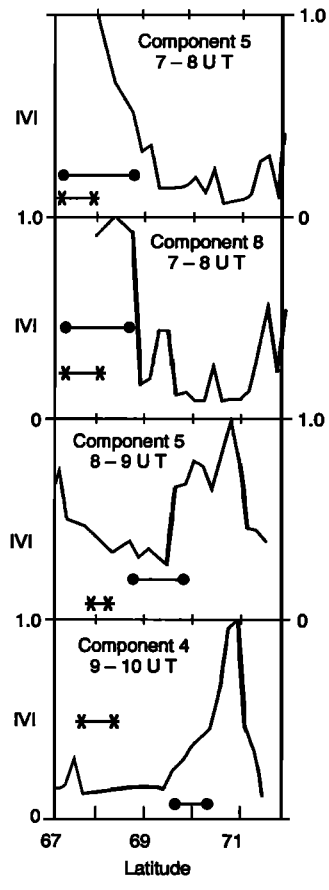

significant at the beginning of the interval. The correlation coefficient in this period (0910 to 1000 hours UT) is around 0.54 at zero lag. With 24 points of data, the correlation is significant at the 99% level. Because of the 10-min periodicity, negative peaks appear in the correlation at lags of ±5 min.

A comparison of Figures 4, 8, and 11 shows that there is a tendency for the region of conjugacy to shift to higher latitudes as the satellite moves outward. This result, which is consistent with our expectations, is brought out more clearly in Figure 12, which depicts, for the relevant modes, the variation of the magnitude of X_{ij} (averaged over longitude bins and then normalized so as to have a maximum value of 1) with latitude. In the 0700–0800 UT interval there are no points below 68°, but there is a clear suggestion of an increase in the amplitude of component 5 toward lower latitudes while component 8 peaks slightly poleward of this limit. At the latitude where component 8 peaks, component 5 has an amplitude which is almost half of its peak value. We note that the satellite was moving outward (and hence from lower to higher latitudes) and that the latitudinal dependence of the components suggests that component 5 should make a larger contribution below 68° and very little above this latitude. It is, therefore, not surprising that the satellite encounters oscillations associated with component 5 before

Fig. 12. Average magnitude of the eigenvector X_{ij} at a given latitude plotted as a function of latitude. Only components whose temporal variations match the AMPTE CCE magnetic field fluctuations are depicted. The amplitudes have been normalized so as to have a maximum value of 1. Conjugate locations based on the dipole (circle line segment) and *Tsyganenko* [1987] (asterisk line segment) models are also presented in the figure.

it enters a region where oscillations are dominated by the mode driving component 8. It should also be noted from Figure 3 that component 5 has a significant amplitude only at the beginning of the time interval. It is also quite clear from Figure 12 that as the satellite moves outward, the region of conjugate oscillations moves to higher latitudes, as expected. The conjugate locations corresponding to the AMPTE CCE locations computed on the basis of a simple dipole model and the *Tsyganenko* [1987] model for the appropriate level of geomagnetic activity are also depicted in the figure. Note that the dipole mapping provides a better fit to the data than the *Tsyganenko* [1987] model. It is quite conceivable that factors that are not adequately represented in the *Tsyganenko* [1987] model, such as field-aligned currents, compensate for some of the distortions produced by distributed magnetospheric currents.

We note from Figures 4, 8, and 11 that the longitudinal extent of the oscillations is quite large and could even extend beyond the field of view of the radar. Thus our method is not suitable for estimating the longitude of the foot of the field line passing through the satellite location. Note that in the event that the satellite is located at a node of the magnetic field oscillation, one would have to use the oscillations in the particle fluxes to identify the conjugacy.

We have looked at the stability of the analysis by changing the size of the intervals as well as the number of locations to be included in the analysis. We find that the nature of the temporal variations does not change appreciably, but the amplitudes need not remain the same. The method, in its current level of sophistication, does not therefore appear suitable for studies that involve comparing the amplitudes at magnetospheric and ionospheric heights. There is, however, considerable scope for refinement of the technique.

7. Summary and Conclusions

We have shown that the multivariate analysis technique adopted by us can, in an objective manner, resolve oscillations in the radar field of view into patterns of independent flows with characteristic spatial and temporal structures. The method can isolate localized flows whose temporal oscillations reproduce salient features of the azimuthal oscillations in the magnetic field recorded at magnetospheric heights by the AMPTE CCE magnetometer. We therefore have a method of tracing the satellite location along magnetic lines of force to ionospheric heights. Problems may be encountered if the spatial structure changes continuously. The number of components required to explain the variations would be considerably enhanced. A particular component may have significant amplitude only in a small segment of time when the spatial structure defined by it matches the mean structure of the oscillations. However, it is also conceivable that the apparent variation of the spatial structure of the oscillation could be reproduced by the superposition of two (or more) modes with stationary spatial structures but with a time-varying amplitude. In such a case our technique could work well. The fact that our analysis has reproduced significant correlations with the AMPTE CCE magnetic field variations in all the intervals shows that moderate geomagnetic activity does not significantly diminish the effectiveness of the method. In this context it should be noted that the technique also offers a powerful method for extracting the natural modes of oscillation in the ionospheric flows, though here it has been used only to study the mapping problem.

We have tacitly assumed in the analysis that the spatial structure of the modes does not change within the interval. We have also not considered the possibility that the wave could be propagating across the field of view. This may account, in part, for the distortion in the observed amplitudes. Furthermore, interpolation could also be carried out over neighboring points for a given time to avoid the distortion of the amplitude structure brought about by the need to interpolate in time.

An analysis based on similar lines but using sliding intervals rather than the fixed intervals adopted here could also be worthwhile as it could be used to trace the satellite movement and changes in the mode of oscillation on a continuous basis. It should be recognized that the patterns of ionospheric flows determined by us are for the intervals as a whole, while the satellite magnetometer records local instantaneous values.

Finally, we note two shortcomings of the technique:

1. The accuracy with which the satellite location can be detected depends on how narrowly the mode is spread in latitude. However, if the extent is too narrow, it may be difficult to establish the similarity. There is also a possibility that some of the components could have similar temporal variation leading to considerable difficulty in the interpretation.

2. There is no simple way of providing a confidence limit on how well the spatial structure is determined. Considerable work needs to be done in this area.

Acknowledgments. We thank K. Takahashi and L. J. Zanetti for providing the programs for reading and plotting the AMPTE CCE data. We are grateful to B. J. Anderson for providing us the routines developed by D. Stern for using the Tsyganenko (1987) model and to D. Stern for permitting us to use them. This work was supported by the National Science Foundation (NSF) Division of Atmospheric Sciences and the Air Force Office of Scientific Research, Directorate of Atmospheric and Chemical Sciences, under NSF grants ATM-8713982 and ATM-9003860.

The Editor thanks N. Lin and another referee for their assistance in evaluating this paper.

References

Anderson, B. J., M. J. Engebretson, S. P. Rounds, L. J. Zanetti, and T. A. Potemra, A statistical study of Pc 3-5 pulsations observed by the AMPTE CCE magnetic fields experiment, 1, Occurrence distributions, *J. Geophys. Res., 95*, 10,495, 1990.

Engebretson, M. J., L. J. Zanetti, T. A. Potemra, and M. H. Acuña, Harmonically structured ULF pulsation observed by AMPTE CCE magnetic field experiment, *Geophys. Res. Lett., 13*, 905, 1986.

Faynberg, E. B., Separation of the geomagnetic field into a normal and an anomalous part, *Geomagn. Aeron., Engl. Transl., 15*, 117, 1975.

Freeman, M. P., J. M. Ruohoniemi, and R. A. Greenwald, The determination of time-stationary two-dimensional convection patterns with single-station radars, *J. Geophys. Res., 96*, 15,735, 1991.

Greenwald, R. A., A. D. M. Walker, and M. Candidi, Use of hydromagnetic waves to map geomagnetic field lines, *J. Geophys. Res., 86*, 11,251, 1981.

Greenwald, R. A., K. B. Baker, R. A. Hutchins, and C. Hanuise, An HF phased-array radar for studying small-scale structure in the high-latitude ionosphere, *Radio Sci., 20*, 63, 1985.

Lin, N. G., L. J. Cahill, Jr., M. J. Engebretson, M. Sugiura, and R. L. Arnoldy, Dayside pulsation event near the plasmapause, *Planet. Space Sci., 34*, 155, 1986.

Potemra, T. A., L. J. Zanetti, and M. H. Acuña, The AMPTE CCE magnetic field experiment, *IEEE Trans. Geosci. Remote Sens., GE-23*, 246, 1985.

Rajaram, M., Method of natural orthogonal components applied to equatorial geomagnetic variations, *Ann. Geophys., 36*, 599, 1980.

Rajaram, M., and R. Rajaram, Wind and temperature structure of the equatorial middle atmosphere, *Indian J. Radio Space Phys., 12*, 160, 1983.

Rao, C. R., The use and interpretation of principal component analysis in applied research, *Sankhya Ser. A, 25*, 359, 1965.

Ruohoniemi, J. M., R. A. Greenwald, K. B. Baker, J. P. Villian, C. Hanuise, and J. Kelly, Mapping high-latitude plasma convection with coherent HF radars, *J. Geophys. Res., 94*, 13,463, 1989.

Ruohoniemi, J. M., R. A. Greenwald, K. B. Baker, and J. C. Samson, HF radar observations of Pc 5 field line resonances in the midnight/early morning sector, *J. Geophys. Res., 96,* 15,697, 1991.

Southwood, D. J., and W. J. Hughes, Theory of hydromagnetic waves in the magnetosphere, *Space Sci. Rev., 35,* 301, 1983.

Stern, D., and I. I. Alexeev, Where do field lines go in the quiet magnetosphere?, *Rev. Geophys., 26,* 782, 1987.

Takahashi, K., R. W. McEntire, A. T. Y. Lui, and T. A. Potemra, Ion flux oscillations associated with radially polarized transverse Pc 5 magnetic pulsation, *J. Geophys. Res., 95,* 3717, 1990.

Tsyganenko, N. A., Global quantitative models of the geomagnetic field in the cislunar magnetosphere for different disturbance levels, *Planet. Space Sci., 35,* 1347, 1987.

K. B. Baker, R. A. Greenwald, R. Rajaram, and J. M. Ruohoniemi, Applied Physics Laboratory, Johns Hopkins University, Johns Hopkins Road, Laurel, MD 20723-6099.

(Received October 1, 1990;
revised February 7, 1992;
accepted March 23, 1992.)